Check for updates

Geophysical Research Letters

RESEARCH LETTER
10.1029/2025GL118856

The Buoyancy of Cratonic Lithospheric Mantle

Z. J. Sudholz[1], A. Copley[1], and K. Priestley[1]

[1]Bullard Labs, Department of Earth Sciences, The University of Cambridge, Cambridge, UK

Abstract Cratons are generally thought to be characterized by stable, long-lived mantle roots. However, recent studies have suggested that the lithospheric mantle may be prone to removal, implying that it may be denser than the asthenosphere. To address these suggestions, we use a global data set of mantle xenoliths to estimate the density structure of the cratonic lithospheric mantle (CLM), which we then compare with the density of the asthenospheric mantle at equivalent depths. Most of the CLM is either neutrally buoyant or slightly positively buoyant relative to the asthenosphere. The exception is where pyroxenite has accumulated due to melt infiltration. For these pyroxenites to remain within the CLM over geologically significant timescales they must be relatively small, that is, ≤1–20 km in size for a CLM viscosity of 10^{21}–10^{23} Pa·s. Our results suggest that the majority of cratonic lithospheric roots are long-lived due to their neutral-to-positive buoyancy.

Plain Language Summary The stability and longevity of mantle roots beneath cratons remain subjects of ongoing debate. While traditionally considered to be stable over billions of years, recent studies have suggested that these roots may be more frequently removed into the underlying mantle than previously thought, a process that would require them to be denser than the surrounding convecting mantle. To address this debate, we have calculated the densities of a global database of mantle-derived xenoliths, at the pressures and temperatures that they equilibrated within the lithospheric mantle, which we then compare with the density of the convecting mantle at equivalent depths. Our results show that the cratonic lithospheric mantle (CLM) sampled by our mantle xenolith data set is dominantly neutrally or positively buoyant with respect to the convecting mantle. Our results therefore show that the buoyancy of the CLM results in its long-term stability, the only exceptions being pyroxenites that have formed by melt infiltration. However, for pyroxenites to have remained in the lithospheric mantle for significant timescales, they must be volumetrically minor.

Key Points:

- Most of the cratonic lithospheric mantle is neutrally or positively buoyant relative to the asthenosphere
- Regions of negative buoyancy develop where pyroxenite has accumulated as a result of melt infiltration
- Pyroxenite bodies must be smaller than 1–20 km to be retained in the lithosphere over geological time scales

Supporting Information:

Supporting Information may be found in the online version of this article.

Correspondence to:

Z. J. Sudholz,
zs441@cam.ac.uk

Citation:

Sudholz, Z. J., Copley, A., & Priestley, K. (2025). The buoyancy of cratonic lithospheric mantle. *Geophysical Research Letters*, *52*, e2025GL118856. https://doi.org/10.1029/2025GL118856

Received 19 AUG 2025
Accepted 3 DEC 2025

Author Contributions:

Conceptualization: Z. J. Sudholz
Formal analysis: Z. J. Sudholz
Funding acquisition: A. Copley
Methodology: Z. J. Sudholz, A. Copley
Supervision: A. Copley, K. Priestley
Writing – original draft: Z. J. Sudholz
Writing – review & editing: Z. J. Sudholz, A. Copley, K. Priestley

© 2025. The Author(s).
This is an open access article under the terms of the Creative Commons Attribution License, which permits use, distribution and reproduction in any medium, provided the original work is properly cited.

1. Introduction

Cratons are generally thought to be long-lived and tectonically-stable fragments of Precambrian continental lithosphere, underlain by thick roots of chemically depleted mantle rocks, including dunite and harzburgite (Lee et al., 2011; Pearson et al., 2021). These rocks were depleted by high-degree partial melting during the Archean and Proterozoic (Pearson et al., 2021). Cratonic lithospheric mantle (CLM) is marked by cooler geothermal gradients and lower heat flow relative to tectonically active regions (Artemieva & Mooney, 2001; Hasterok & Chapman, 2011). The long-term stability of CLM has been suggested to be facilitated by its distinct thermal structure and chemical composition; the increased density relative to the asthenosphere due to its cooler temperature is offset by the lower densities caused by the depleted mantle compositions (Jordan, 1975, 1988; Lee, 2003). These properties allow cratons to remain neutrally buoyant (isopycnic) with respect to the asthenosphere, limiting their susceptibility to removal into the convecting mantle. Moreover, their depleted compositions limit re-melting to localized, volatile-enriched (metasomatized) zones that typically produce only small melt volumes (e.g., Foley, 1992; Prelević et al., 2024). Geophysical and petrological data indicate that most cratons have maintained a nearly constant lithospheric thickness since at least the Paleoproterozoic (Sudholz & Copley, 2025; Sudholz, Priestley, & Copley, 2025). Radiogenic Re–Os isotope systematics further imply that most cratons have remained geochemically and mechanically isolated from mantle convection for over 2 billion years (Pearson et al., 2021 refs therein). This interpretation is also supported by numerical modeling, which attributes cratonic stability to their thick, strong (high viscosity), melt-depleted roots (e.g., Lenardic et al., 2003; Wang et al., 2014). However, recent studies have suggested an alternative view, that the destruction and destabilization of the CLM may be more common than previously thought (Gernon et al., 2023; Hoare et al., 2022; Hu et al., 2018; Sarkar et al., 2025; Stephenson et al., 2023). Such a process implies that the CLM must possess sufficient density to be removed and incorporated into the asthenosphere. Resolving uncertainties surrounding the density, and therefore

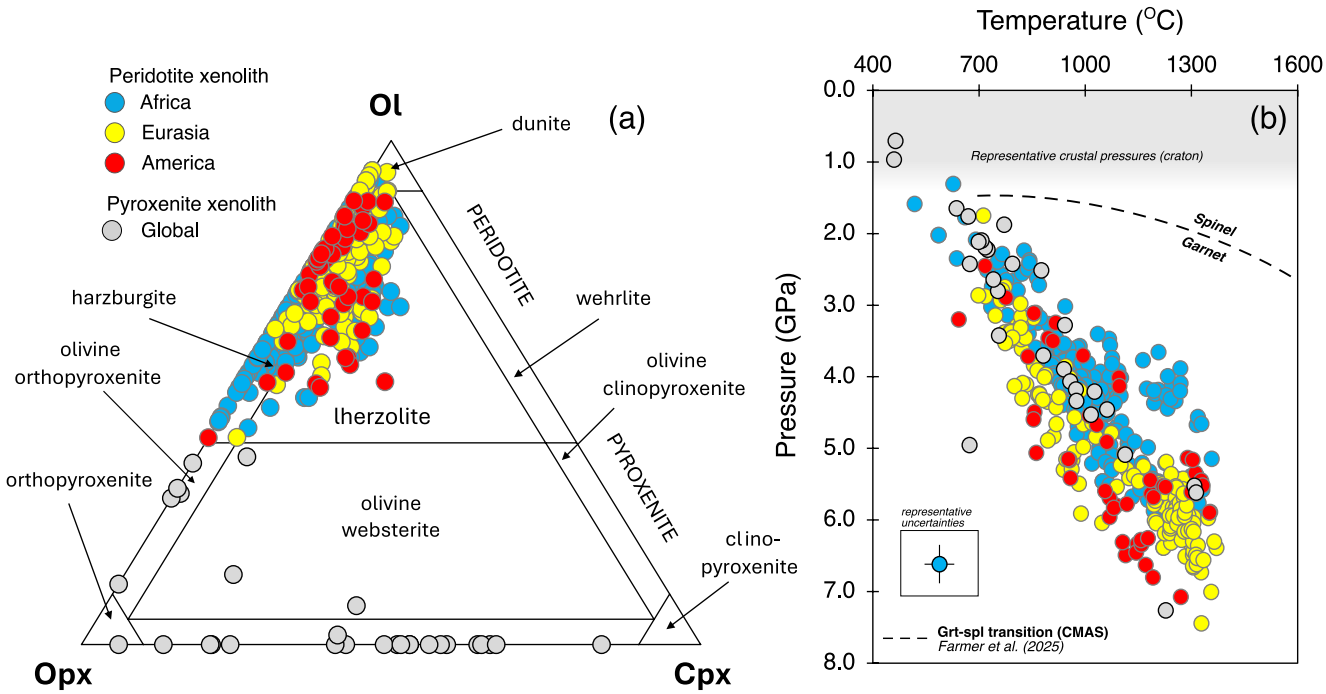

Figure 1. Mineralogy and equilibration P–T of xenoliths. (a) Ternary diagram showing the modal mineralogy and rock types of the xenoliths used in the study. (b) Diagram showing the P–T range of the xenoliths. Garnet-spinel transition (dashed line) is from Farmer et al. (2025) for the CaO-MgO-Al_2O_3-SiO_2 (CMAS) system. Inset shows the representative uncertainty on P-T estimates. The shaded region is the approximate pressure range (in GPa) of the continental crust within cratons. Ol is olivine. Opx is orthopyroxene. Cpx is clinopyroxene.

long-term stability, of the CLM is essential for our understanding of craton evolution and its influence on magmatism, resource distribution, and global climate and volatile cycles (Cawood et al., 2022; Pearson et al., 2021).

In this study we assess the density of the CLM by analyzing the pressure–temperature–density–composition (P–T–ρ–X) of 497 mantle xenoliths. For each xenolith, we estimate density at the P–T of equilibration and compare it with asthenospheric density estimates at corresponding depths based on phase equilibria modeling of fertile peridotite along a mantle isentrope. This approach enables us to investigate how variations in pressure, temperature and composition affect the density profile—and, by extension, the long-term stability—of the CLM. Finally, we use a dynamic model to examine the spatial scale of high-density lithologies that would allow them to survive for billions of years within the CLM.

2. Method: Xenolith Data Set

To estimate the density structure of the CLM, we use a global data set of mantle xenoliths (see Sudholz, Copley, and Priestley (2025) for data). This data set of published analyses includes modal mineral proportions and compositions for 497 samples. It includes compilations by Nimis and Grütter (2010), Tomlinson and Kamber (2021), and Sudholz and Copley (2025). The xenoliths were sourced from kimberlites and related volcanic rocks occurring within cratons and craton margins (Supporting Information S1) and have eruption ages of 20–1,150 Ma. The compilation includes samples from most major cratons including Kaapvaal, Slave, and Siberia. Lithologies in the data set include garnet-bearing orthopyroxenites, websterites, harzburgites, lherzolites, and wehrlites (Figure 1a). Spinel-facies xenoliths and dunites were excluded from our analysis due to the lack of suitable geobarometers. The exclusion of spinel-only peridotites has no significant effect on our results due to their narrow pressure range of stability between typical Moho pressures (~1.1–1.3 GPa, for crustal thicknesses of 40–45 km and densities of 2,800–2,900 kg/m^3), and the first appearance of garnet at the relevant temperatures (~1.5 GPa), as shown on Figure 1b (e.g., Farmer et al., 2025). The compositions of primary minerals were filtered to only include high-quality analyses (i.e., 98–102 wt% oxide total). Given the range in xenolith lithologies, equilibration P–T were estimated using multiple geothermobarometers. For four-phase lherzolites, we applied the Taylor (1998) two-pyroxene solvus geothermometer and the Nickel and Green (1985) garnet–orthopyroxene

19448007, 2025, 24, Downloaded from https://agupubs.onlinelibrary.wiley.com/doi/10.1029/2025GL118856 by Cambridge University Library, Wiley Online Library on [17/12/2025]. See the Terms and Conditions (https://onlinelibrary.wiley.com/terms-and-conditions) on Wiley Online Library for rules of use; OA articles are governed by the applicable Creative Commons License

19448007, 2025, 24, Downloaded from https://agupubs.onlinelibrary.wiley.com/doi/10.1029/2025GL118856 by Cambridge University Library, Wiley Online Library on [17/12/2025]. See the Terms and Conditions (https://onlinelibrary.wiley.com/terms-and-conditions) on Wiley Online Library for rules of use; OA articles are governed by the applicable Creative Commons License

geobarometer. For garnet-bearing harzburgites, the Sudholz et al. (2022) garnet–orthopyroxene Fe–Mg exchange geothermometer and the Nickel and Green (1985) garnet–orthopyroxene geobarometer were used. The uncertainties across all geothermobarometers range from 35°C to 75°C and 0.25–0.50 GPa. The mineral compositions and modal abundances of each xenolith were used to estimate the proportions of the mineral end-members (see Sudholz, Copley, and Priestley (2025) for data). The end-member proportions, combined with P–T estimates, were used to calculate the density of each xenolith using the program developed by Abers and Hacker (2016). This program is a MATLAB toolbox and Excel workbook that calculates the physical properties of rocks, including density, based on the proportions of mineral end-members and the P–T conditions. The uncertainty on density estimates for well characterized mineral end-members, such as those found in peridotite xenoliths, are typically <0.50% of the bulk xenolith density (Hacker et al., 2003; Schutt & Lesher, 2006). Because this method depends on mineral composition and mineral modal abundance (rather than whole-rock composition; WR), it can be applied to xenoliths that have experienced complex melting and metamorphic histories. Further details of the method is provided in Hacker and Abers (2004) and Abers and Hacker (2016). Taken together, the cumulated uncertainties in our density estimates related to equilibration conditions and calculation of the physical parameters are less than 20 kg/m^3 (see Sudholz, Copley, and Priestley (2025) for data), and we do not expect our results to be systematically biased toward over- or under-estimates. Using this method, our xenolith data set provides the necessary parameters (P–T–ρ–X) to investigate the density structure of the CLM.

3. Method: Ambient Mantle Density Structure

To assess the buoyancy of the CLM, it is necessary to also calculate the density structure of the asthenosphere over an equivalent depth range, so that they can be compared. We use the equilibration pressures of each xenolith (0.71–7.5 GPa) and estimate the depth-equivalent temperature of the asthenosphere along a mantle isentrope (with a fixed mantle potential temperature (Tp) of 1315°C). The equilibration pressures of the xenoliths were converted to depth using a crustal thickness and density of 40 km and 2,800 kg/m^3 (James et al., 2003; Kozlovskaya et al., 2008; Snyder et al., 2014) and the mantle lithosphere density estimated for the xenolith in question. Using a constant mantle lithosphere density has minimal effects on our results, due to the small percentages changes in density we estimate here. The estimated depths of the xenoliths would change by <5 km if we used alternative geologically plausible values for the crust within ±5 km thickness and ±100 kg/m^3 crustal density. The estimated xenolith depths were then used to calculate the depth-equivalent temperatures along the 1315°C isentrope. A modern-day value of Tp of 1315°C was used based on the justification provided by Sudholz and Copley (2025). Density estimates using a higher Tp of 1415°C are discussed below. The temperature along the isentrope (Tp = 1315°C) for the depth range of the xenoliths is 1324°C–1438°C. Based on this P–T range (1324°C–1438°C and 0.71–7.5 GPa), the density of the asthenospheric mantle was calculated using the MAGEMin Gibbs Energy Minimizer software (version 1.6.6, Riel et al., 2022), in conjunction with the thermodynamic models of Green et al. (2025) and the ds62 data set of Holland and Powell (2011). Calculations were performed using a representative anhydrous fertile mantle composition (KLB-1) (see Supporting Information S1). KLB-1 is a widely used natural analog for the composition of the fertile upper mantle (Davis et al., 2009). This density calculation involves converting depth to pressure, for which we used the same crustal parameters as given above (so any uncertainties affect both calculations equally), and a mantle density calculated for KLB-1.

To ensure consistency between the two methods for estimating density (i.e., Abers & Hacker, 2016 and MAGEMin, Riel et al., 2022), we conducted tests on well-equilibrated xenoliths with reported mineral modes and whole-rock (WR) oxide compositions. The samples in this test data set (n = 51) record a wide range of mineral modes that reflect highly depleted and fertile compositions. When applied to these samples, both methods yielded almost identical density estimates when applied to the same rock and P-T conditions. The differences between densities estimated using the two methods were dominantly <10 kg/m^3, with a mean of 4.87 kg/m^3 (Supporting Information S1). We show below that this value is small compared to our estimated differences between CLM and asthenosphere densities, meaning that our comparison is accurate and the calculated density contrasts are reliable, and not due to methodological biases.

4. Results and Discussion

The equilibration P–T of the xenoliths range between 460°C and 1371°C and 0.71–7.5 GPa (Figure 1b). P–T estimates from the different geothermobarometer calibrations typically agree within ±50°C and ±0.25–0.50 GPa (see Sudholz, Copley, and Priestley (2025) for data) Peridotite and pyroxenite xenoliths returned P–T

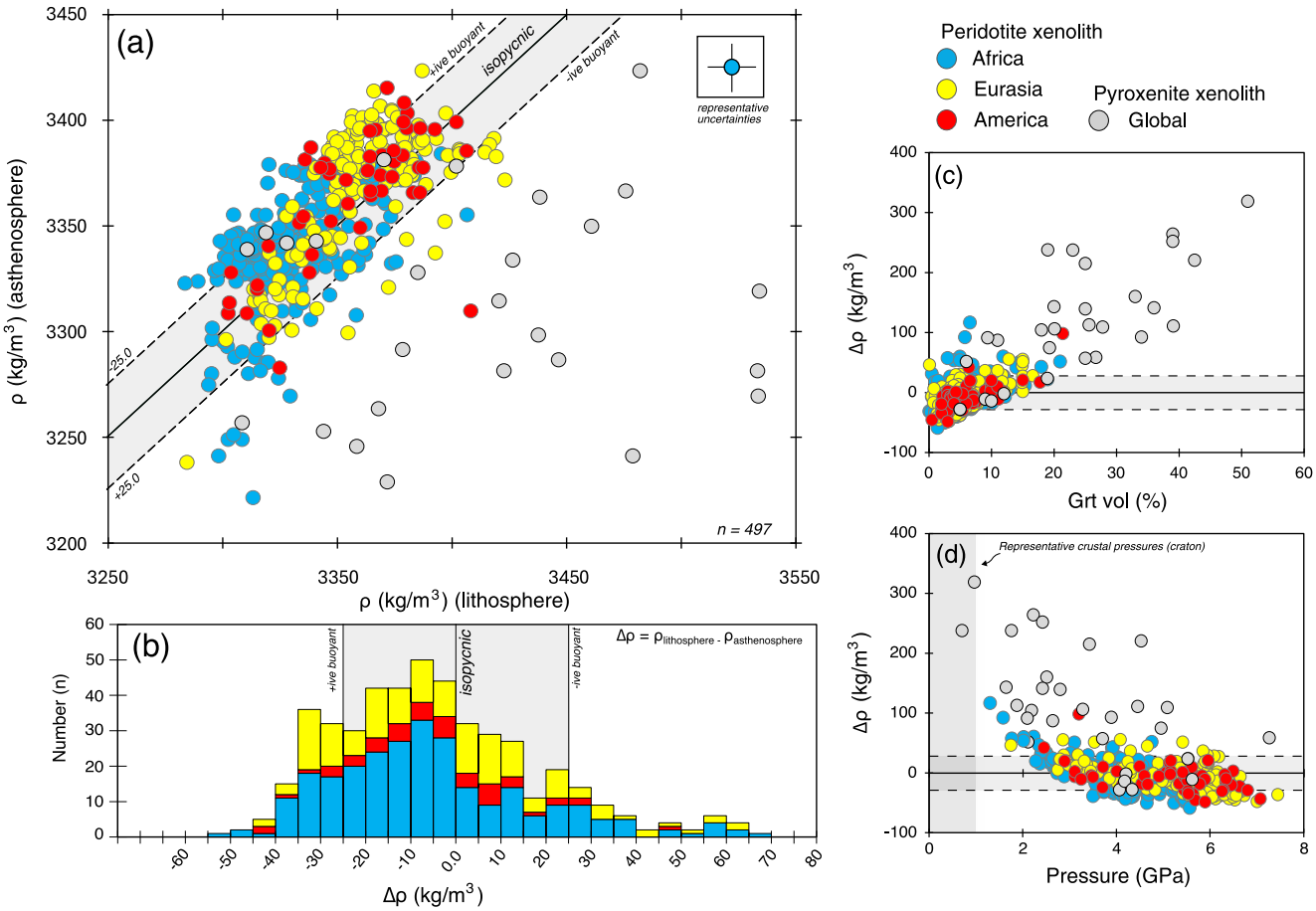

Figure 2. Trends in the P–T–$\Delta\rho$–X ($\Delta\rho = \rho_{\text{lithosphere}} - \rho_{\text{asthenosphere}}$) of the xenoliths. (a) Diagram showing the density (ρ) of the xenoliths (x-axis, lithosphere) plotted against the density (ρ) of the asthenosphere at the same depth (km) along the mantle isentrope (Tp = 1315°C). See Methods for further details. Inset shows the representative uncertainty on the density estimates. (b) Histogram showing the difference ($\Delta\rho$) in density for peridotite xenoliths calculated at their equilibration P–T with the density of asthenosphere calculated at the same depth along the mantle isentrope. Bin size is 5 kg/m^3. (c) $\Delta\rho$ plot against garnet volume (%) for each xenolith. (d) $\Delta\rho$ plot against the equilibration pressure (GPa) for each xenolith.

estimates covering most of the CLM. The calculated densities of peridotite xenoliths at their equilibration P–T conditions ranged from 3,284 to 3,423 kg/m^3, while those of pyroxenite xenoliths ranged from 3,308 to 3,572 kg/m^3. Peridotite xenoliths with elevated modal orthopyroxene (i.e., opx-enrichment) record similar densities to unenriched samples. This trend was also reported by Schutt and Lesher (2010). Xenolith densities calculated at standard P–T (STP) are also reported in Supporting Information S1, which isolates the effect of composition on the density. This comparison shows a range in density from compositional effects alone that is mostly within 100 kg/m^3, with a standard deviation of 37.5 kg/m^3. These values agree well with the compositional density differences between lithospheric mantle and the convecting mantle of ~50–60 kg/m^3 estimated by McKenzie and Priestley (2016) on the basis of the compositions of mantle-derived magmas.

Comparison of xenolith densities with asthenospheric densities at equivalent depths along the isentrope ($\Delta\rho = \rho_{\text{lithosphere}} - \rho_{\text{asthenosphere}}$) reveals several trends. Figures 2a and 2b show that most peridotite xenoliths have densities that are similar to, or slightly below, asthenospheric densities at equivalent depths, over the wide depth range sampled by our data set (Figure 2d). This pattern strongly supports the interpretation that the CLM is predominantly neutrally buoyant or slightly positively buoyant (Jordan, 1975, 1988). Slight positive density differences within the shallow CLM (<3 GPa) may imply that this region is not entirely isopycnic. This observation was also pointed out by Schutt and Lesher (2006). Notwithstanding, the broadly isopycnic to positively buoyant nature of the CLM across the depth range of our xenolith data set, as evidenced from our Figures 2a and 2b results, challenges several recent studies which have questioned the long-term stability and

19448007, 2025, 24, Downloaded from https://agupubs.onlinelibrary.wiley.com/doi/10.1029/2025GL118856 by Cambridge University Library, Wiley Online Library on [17/12/2025]. See the Terms and Conditions (https://onlinelibrary.wiley.com/terms-and-conditions) on Wiley Online Library for rules of use; OA articles are governed by the applicable Creative Commons License

19448007, 2025, 24, Downloaded from https://agupubs.onlinelibrary.wiley.com/doi/10.1029/2025GL118856 by Cambridge University Library, Wiley Online Library on [17/12/2025]. See the Terms and Conditions (https://onlinelibrary.wiley.com/terms-and-conditions) on Wiley Online Library for rules of use; OA articles are governed by the applicable Creative Commons License

density structure of the CLM (e.g., Gernon et al., 2023; Hoare et al., 2022; Hu et al., 2018; Sarkar et al., 2025; Stephenson et al., 2023).

Figure S10 in Supporting Information S1 shows the results of our calculation if a higher mantle potential temperature (1415°C) is used for the calculation of asthenosphere density, although we note that the actual changes in potential temperature are likely to be much lower over the 20–1,150 Ma time interval covered by our xenolith eruption ages (for the reasons outlined in Sudholz & Copley, 2025). However, even using this distinctly hotter mantle our results remain unchanged, with the density differences experiencing only a shift of ∼12.5 kg/m^3 toward less-buoyant lithosphere, due to the hotter ambient mantle. This shift is insufficient to alter the main patterns in the data, which are instead governed by compositional effects (Figure 2). Additionally, this hypothetical scenario does not consider the counteracting effect of the lithospheric mantle being warmer due to heat transfer with the asthenosphere—an effect that would be made invisible in the xenolith data set by subsequent re-equilibration before eruption, and so not included in this calculation.

An exception to the neutrally to-positively buoyant density structure of the CLM, as revealed by our xenoliths, is observed for pyroxenites (Figure 2a). These samples mostly have higher densities than the asthenosphere at equivalent depths, largely due to their higher modal garnet contents (Figure 2c). The presence of these dense lithologies within the xenolith data set implies that the spread of densities we have observed is not governed by any hypothetical inability of kimberlites and related rocks to entrain dense lithologies—xenoliths with densities greater than 3,500 kg/m^3 at their equilibration P–T conditions show that even very dense lithologies are able to be entrained and erupted. Most pyroxenites in our data set are high-MgO varieties (i.e., Lee et al., 2011). These rocks are not eclogites, due to their elevated orthopyroxene contents and lack of omphacite (see Sudholz, Copley, and Priestley (2025) for data). The elevated Cr_2O_3 contents and lower CaO in garnet is also inconsistent with these rocks being eclogites. High-MgO pyroxenites are thought to represent one or more of: (a) subducted picritic oceanic crust, (b) the products of melt-rock reaction between basaltic liquids and peridotite, (c) trapped high-pressure mantle-derived liquids, or (d) high-pressure cumulates (Lee et al., 2011 refs therein). The elevated garnet content and higher concentrations of FeO and Al_2O_3 in pyroxenes and garnets relative to peridotitic assemblages indicate that these rocks formed through refertilization by melt infiltration. The formation of pyroxenites within the CLM locally increased the density of the lithospheric mantle. These results are consistent with previous studies, which have highlighted the role of pyroxenite and related metasomatic lithologies in increasing the density of the CLM (e.g., Aitken et al., 2023; Dai et al., 2021; Kelly et al., 2003; Schutt & Lesher, 2010; Zheng et al., 2015).

The number of pyroxenite xenoliths, and their density contrast with respect to the peridotites and the asthenosphere, both imply that they form a volumetrically minor component of the CLM. Over time, dense pyroxenites will sink through, and be removed from, the CLM due to their negative buoyancy (Lee et al., 2011). However, the xenolith record shows that some pyroxenite bodies were present within the CLM at the time of eruption. To quantify the physical conditions that are compatible with the presence of these lithospheric pyroxenites, Figure 3 shows calculations for the velocity at which more-dense pyroxenite would sink through less-dense peridotite mantle, as a function of the density difference between them, the viscosity of the peridotite mantle, and the radius of the pyroxenite body. These calculations were performed by modeling the pyroxenite body as a sphere, with a negligible viscosity, using the expressions given in Batchelor (1967). Other geometries, or higher viscosities for the pyroxenite, would result in slower sinking velocities. The bold contour on Figure 3 shows the velocity required to sink through 100 km of lithospheric mantle in 3 Gyr. The viscosity of the lithospheric mantle is not well known, but a lower bound is provided by the viscosity of the (hotter) convecting upper mantle (10^{21} Pa·s, Lau et al., 2018; Peltier, 1996). An estimate of 10^{23} Pa·s was suggested by Priestley and McKenzie (2013) based upon the seismic characteristics of the mantle lithosphere. The results on Figure 3 show that for pyroxenites to be stable over geologically significant time periods requires them to be present as bodies smaller than ∼1–20 km, for a viscosity of 10^{21}–10^{23} Pa·s, suggesting that they are small (and therefore volumetrically minor) components of the cratonic mantle. These results agree with the observations from ophiolite complexes, which show that pyroxenite layers typically occur on length-scales of a tens of meters to millimeters (see Sudholz, Copley, and Priestley (2025) for data), although it is unclear whether these regions would be expected to have similar geometries to the CLM. A reduction of an order of magnitude in the density difference used in the calculations, as would be relevant for the differences between the varied peridotite lithologies (Figures 2a and 2b) would reduce the sinking velocity by an order of magnitude. These density differences are therefore insufficient to generate density-sorting within the peridotites over the age of the Earth under these viscosity conditions. This finding is consistent with the

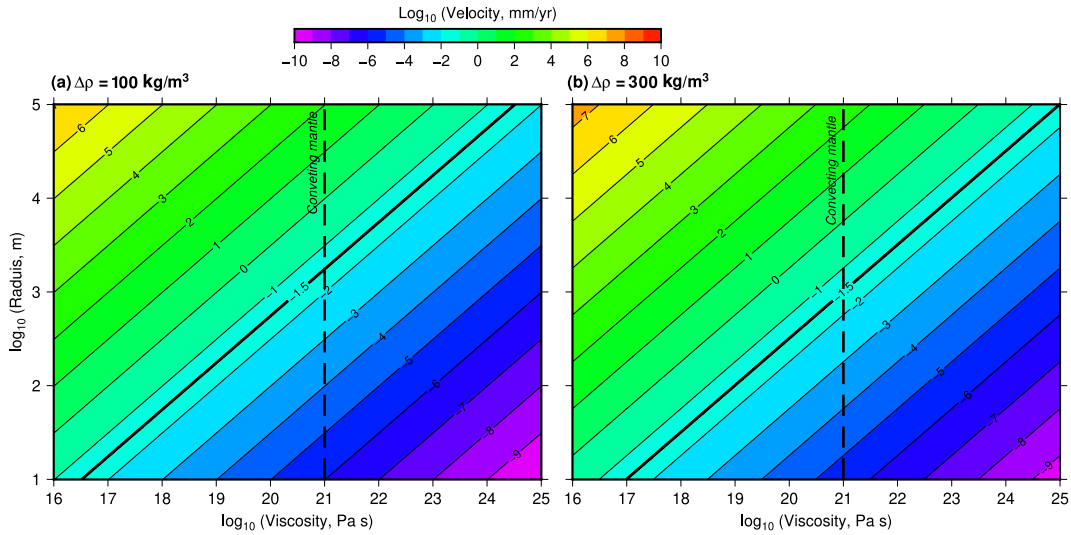

Figure 3. The velocity at which a more-dense pyroxenite body will sink through less-dense ambient lithospheric mantle, as a function of the viscosity of the ambient mantle and the radius of the body. Calculations are shown for density differences of (a) 100 and (b) 300 kg/m^3. Dashed line shows a likely viscosity for the convecting mantle, and the bold contour (0.03 mm/yr) shows the velocity required to sink by ∼100 km over ∼3 Gyr.

observation of seismically imaged structures within the lithospheric mantle that are interpreted to have persisted for billions of years since formation (e.g., Clowes et al., 2010).

5. Conclusion

A global data set of mantle xenoliths has been used to model the density structure of the CLM. For each xenolith, lithospheric density estimates were compared with estimates of asthenospheric density at equivalent depths. Cratons typically have a density structure that is neutrally to-positively buoyant with respect to the asthenosphere. Deviations in this trend occur in regions where pyroxenite has accumulated due to melt infiltration and refertilization. These rocks increased the density of the lithosphere by >100 kg/m^3. Dynamic models show that for these pyroxenites to be stable over geologically significant time periods requires them to be in bodies smaller than ∼1–20 km, for a viscosity of 10^{21}–10^{23} Pa·s. Our results support the concept that cratonic lithospheric mantle roots are long-lived stable features because of their buoyancy relative to the convecting mantle.

Conflict of Interest

The authors declare no conflicts of interest relevant to this study.

Data Availability Statement

All data used in this study is provided in the Supporting Information S1 and in the Zenodo data repository of Sudholz, Copley, and Priestley (2025) (10.5281/zenodo.17839124).

Acknowledgments
This work was funded by NERC Grant NE/W00562X/1. P–T estimates were made using PTEXL (https://cms.eas.ualberta.ca/team-diamond/downloads/). Paolo Nimis is thanked for providing some of the xenolith analyses used in this study. James Jackson is thanked for discussions. Derek Schutt and one anonymous reviewer are thanked for their detailed comments which helped improve the manuscript. Quentin Williams is thanked for editorial handling.

References

Abers, G. A., & Hacker, B. R. (2016). A MATLAB toolbox and Excel workbook for calculating the densities, seismic wave speeds, and major element composition of minerals and rocks at pressure and temperature. *Geochemistry, Geophysics, Geosystems*, *17*(2), 616–624. https://doi.org/10.1002/2015gc006171

Aitken, A. R. A., Fiorentini, M., Tesauro, M., & Thébaud, N. (2023). Supercontinent-paced magmatic destabilisation and recratonisation of the Yilgarn Craton. *Gondwana Research*, *116*, 12–24. https://doi.org/10.1016/j.gr.2022.11.016

Artemieva, I. M., & Mooney, W. D. (2001). Thermal thickness and evolution of Precambrian lithosphere: A global study. *Journal of Geophysical Research*, *106*(B8), 16387–16414. https://doi.org/10.1029/2000jb900439

Batchelor, G. K. (1967). *An introduction to fluid dynamics*. Cambridge University Press.

Cawood, P. A., Chowdhury, P., Mulder, J. A., Hawkesworth, C. J., Capitanio, F. A., Gunawardana, P. M., & Nebel, O. (2022). Secular evolution of continents and the Earth system. *Reviews of Geophysics*, *60*(4), e2022RG000789. https://doi.org/10.1029/2022rg000789

Clowes, R. M., White, D. J., & Hajnal, Z. (2010). Mantle heterogeneities and their significance: Results from lithoprobe seismic reflection and refraction–wide-angle reflection studies. *Canadian Journal of Earth Sciences*, *47*(4), 409–443. https://doi.org/10.1139/e10-009

19448007, 2025, 24, Downloaded from https://agupubs.onlinelibrary.wiley.com/doi/10.1029/2025GL118856 by Cambridge University Library, Wiley Online Library on [17/12/2025]. See the Terms and Conditions (https://onlinelibrary.wiley.com/terms-and-conditions) on Wiley Online Library for rules of use; OA articles are governed by the applicable Creative Commons License

Dai, H. K., Zheng, J. P., Griffin, W. L., O'Reilly, S. Y., Xiong, Q., Ping, X. Q., et al. (2021). Pyroxenite xenoliths record complex melt impregnation in the deep lithosphere of the northwestern North China Craton. *Journal of Petrology*, *62*(2), egaa079. https://doi.org/10.1093/petrology/egaa079

Davis, F. A., Tangeman, J. A., Tenner, T. J., & Hirschmann, M. M. (2009). The composition of KLB-1 peridotite. *American Mineralogist*, *94*(1), 176–180. https://doi.org/10.2138/am.2009.2984

Farmer, N., O'Neill, H. S. C., & Green, E. C. (2025). The spinel to garnet phase transition in the systems MgO-Al_2O_3-SiO_2 and CaO-MgO-Al_2O_3-SiO_2: New experiments to resolve long-standing discrepancies. *Contributions to Mineralogy and Petrology*, *180*(2), 14. https://doi.org/10.1007/s00410-025-02203-x

Foley, S. (1992). Vein-plus-wall-rock melting mechanisms in the lithosphere and the origin of potassic alkaline magmas. *Lithos*, *28*(3–6), 435–453. https://doi.org/10.1016/0024-4937(92)90018-t

Gernon, T. M., Jones, S. M., Brune, S., Hincks, T. K., Palmer, M. R., Schumacher, J. C., et al. (2023). Rift-induced disruption of cratonic keels drives kimberlite volcanism. *Nature*, *620*(7973), 344–350. https://doi.org/10.1038/s41586-023-06193-3

Green, E. C., Holland, T. J., Powell, R., Weller, O. M., & Riel, N. (2025). Corrigendum to: Melting of peridotites through to granites: A simple thermodynamic model in the system KNCFMASHTOCr, and, a thermodynamic model for the subsolidus evolution and melting of peridotite. *Journal of Petrology*, *66*(1), egae079. https://doi.org/10.1093/petrology/egae079

Hacker, B. R., & Abers, G. A. (2004). Subduction factory 3: An Excel worksheet and macro for calculating the densities, seismic wave speeds, and H_2O contents of minerals and rocks at pressure and temperature. *Geochemistry, Geophysics, Geosystems*, *5*(1), Q01005. https://doi.org/10.1029/2003gc000614

Hacker, B. R., Abers, G. A., & Peacock, S. M. (2003). Subduction factory 1. Theoretical mineralogy, densities, seismic wave speeds, and H_2O contents. *Journal of Geophysical Research*, *108*(B1), 2029. https://doi.org/10.1029/2001jb001127

Hasterok, D., & Chapman, D. S. (2011). Heat production and geotherms for the continental lithosphere. *Earth and Planetary Science Letters*, *307*(1–2), 59–70. https://doi.org/10.1016/j.epsl.2011.04.034

Hoare, B. C., Tomlinson, E. L., & Kamber, B. S. (2022). Evidence for a very thick Kaapvaal craton root: Implications for equilibrium fossil geotherms in the early continental lithosphere. *Earth and Planetary Science Letters*, *597*, 117796. https://doi.org/10.1016/j.epsl.2022.117796

Holland, T. J. B., & Powell, R. (2011). An improved and extended internally consistent thermodynamic dataset for phases of petrological interest, involving a new equation of state for solids. *Journal of Metamorphic Geology*, *29*(3), 333–383. https://doi.org/10.1111/j.1525-1314.2010.00923.x

Hu, J., Liu, L., Faccenda, M., Zhou, Q., Fischer, K. M., Marshak, S., & Lundstrom, C. (2018). Modification of the Western Gondwana craton by plume–lithosphere interaction. *Nature Geoscience*, *11*(3), 203–210. https://doi.org/10.1038/s41561-018-0064-1

James, D. E., Niu, F., & Rokosky, J. (2003). Crustal structure of the Kaapvaal craton and its significance for early crustal evolution. *Lithos*, *71*(2–4), 413–429. https://doi.org/10.1016/j.lithos.2003.07.009

Jordan, T. H. (1975). The continental tectosphere. *Reviews of Geophysics*, *13*(3), 1–12. https://doi.org/10.1029/rg013i003p00001

Jordan, T. H. (1988). Structure and formation of the continental tectosphere. *Journal of Petrology*, (1), 11–37. https://doi.org/10.1093/petrology/special_volume.1.11

Kelly, R. K., Kelemen, P. B., & Jull, M. (2003). Buoyancy of the continental upper mantle. *Geochemistry, Geophysics, Geosystems*, *4*(2), 1017. https://doi.org/10.1029/2002gc000399

Kozlovskaya, E., Kosarev, G., Aleshin, I., Riznichenko, O., & Sanina, I. (2008). Structure and composition of the crust and upper mantle of the Archean–Proterozoic boundary in the Fennoscandian shield obtained by joint inversion of receiver function and surface wave phase velocity of recording of the SVEKALAPKO array. *Geophysical Journal International*, *175*(1), 135–152. https://doi.org/10.1111/j.1365-246x.2008.03876.x

Lau, H. C. P., Austermann, J., Mitrovica, J. X., Crawford, O., Al-Attar, D., & Latychev, K. (2018). Inferences of mantle viscosity based on ice age data sets: The bias in radial viscosity profiles due to the neglect of laterally heterogeneous viscosity structure. *Journal of Geophysical Research: Solid Earth*, *123*(9), 7237–7252. https://doi.org/10.1029/2018jb015740

Lee, C. T. A. (2003). Compositional variation of density and seismic velocities in natural peridotites at STP conditions: Implications for seismic imaging of compositional heterogeneities in the upper mantle. *Journal of Geophysical Research*, *108*(B9).

Lee, C. T. A., Luffi, P., & Chin, E. J. (2011). Building and destroying continental mantle. *Annual Review of Earth and Planetary Sciences*, *39*(1), 59–90. https://doi.org/10.1146/annurev-earth-040610-133505

Lenardic, A., Moresi, L. N., & Mühlhaus, H. (2003). Longevity and stability of cratonic lithosphere: Insights from numerical simulations of coupled mantle convection and continental tectonics. *Journal of Geophysical Research*, *108*(B6), 2303. https://doi.org/10.1029/2002jb001859

McKenzie, D., & Priestley, K. (2016). Speculations on the formation of cratons and cratonic basins. *Earth and Planetary Science Letters*, *435*, 94–104. https://doi.org/10.1016/j.epsl.2015.12.010

Nickel, K. G., & Green, D. H. (1985). Empirical geothermobarometry for garnet peridotites and implications for the nature of the lithosphere, kimberlites and diamonds. *Earth and Planetary Science Letters*, *73*(1), 158–170. https://doi.org/10.1016/0012-821x(85)90043-3

Nimis, P., & Grütter, H. (2010). Internally consistent geothermometers for garnet peridotites and pyroxenites. *Contributions to Mineralogy and Petrology*, *159*(3), 411–427. https://doi.org/10.1007/s00410-009-0455-9

Pearson, D. G., Scott, J. M., Liu, J., Schaeffer, A., Wang, L. H., van Hunen, J., et al. (2021). Deep continental roots and cratons. *Nature*, *596*(7871), 199–210. https://doi.org/10.1038/s41586-021-03600-5

Peltier, W. R. (1996). Mantle viscosity and ice-age ice sheet topography. *Science*, *273*(5280), 1359–1364. https://doi.org/10.1126/science.273.5280.1359

Prelević, D., Förster, M. W., Buhre, S., Gülmez, F., Grützner, T., Wang, Y., & Foley, S. F. (2024). Recent advances made by reaction experiments on melting of heavily metasomatized hydrous mantle. *Earth-Science Reviews*, *256*, 104881. https://doi.org/10.1016/j.earscirev.2024.104881

Priestley, K., & McKenzie, D. (2013). The relationship between shear wave velocity, temperature, attenuation and viscosity in the shallow part of the mantle. *Earth and Planetary Science Letters*, *381*, 78–91. https://doi.org/10.1016/j.epsl.2013.08.022

Riel, N., Kaus, B. J., Green, E. C. R., & Berlie, N. (2022). MAGEMin, an efficient Gibbs energy minimizer: Application to igneous systems. *Geochemistry, Geophysics, Geosystems*, *23*(7), e2022GC010427. https://doi.org/10.1029/2022gc010427

Sarkar, S., Giuliani, A., Dalton, H., Munch, F., Phillips, D., & Ghosh, S. (2025). Testing the hypothesis of secular thinning and compositional evolution of the lithospheric mantle beneath cratons: Implications for kimberlite magmatism. *Mineralogy and Petrology*, *119*(4), 1–15. https://doi.org/10.1007/s00710-025-00924-2

Schutt, D. L., & Lesher, C. E. (2006). Effects of melt depletion on the density and seismic velocity of garnet and spinel lherzolite. *Journal of Geophysical Research*, *111*(B5), B05401. https://doi.org/10.1029/2003jb002950

Schutt, D. L., & Lesher, C. E. (2010). Compositional trends among Kaapvaal Craton garnet peridotite xenoliths and their effects on seismic velocity and density. *Earth and Planetary Science Letters*, *300*(3–4), 367–373. https://doi.org/10.1016/j.epsl.2010.10.018

19448007, 2025, 24, Downloaded from https://agupubs.onlinelibrary.wiley.com/doi/10.1029/2025GL118856 by Cambridge University Library, Wiley Online Library on [17/12/2025]. See the Terms and Conditions (https://onlinelibrary.wiley.com/terms-and-conditions) on Wiley Online Library for rules of use; OA articles are governed by the applicable Creative Commons License

Snyder, D. B., Hillier, M. J., Kjarsgaard, B. A., De Kemp, E. A., & Craven, J. A. (2014). Lithospheric architecture of the slave craton, northwest Canada, as determined from an interdisciplinary 3-D model. *Geochemistry, Geophysics, Geosystems*, *15*(5), 1895–1910. https://doi.org/10.1002/2013gc005168

Stephenson, S. N., Ball, P. W., & Richards, F. D. (2023). Destruction and regrowth of lithospheric mantle beneath large igneous provinces. *Science Advances*, *9*(36), eadf6216. https://doi.org/10.1126/sciadv.adf6216

Sudholz, Z. J., & Copley, A. (2025). Xenolith constraints on the mantle potential temperature and thickness of cratonic roots through time. *Geophysical Research Letters*, *52*(2), e2024GL112851. https://doi.org/10.1029/2024gl112851

Sudholz, Z. J., Copley, A., & Priestley, K. F. (2025). Buoyancy of cratonic lithospheric mantle [Dataset]. *Zenodo*. https://doi.org/10.5281/zenodo.17839124

Sudholz, Z. J., Green, D. H., Yaxley, G. M., & Jaques, A. L. (2022). Mantle geothermometry: Experimental evaluation and recalibration of Fe–Mg geothermometers for garnet-clinopyroxene and garnet-orthopyroxene in peridotite, pyroxenite and eclogite systems. *Contributions to Mineralogy and Petrology*, *177*(8), 77. https://doi.org/10.1007/s00410-022-01944-3

Sudholz, Z. J., Priestley, K. F., & Copley, A. (2025). Long-term evolution, stability, and thickness of cratonic lithosphere. *Geology*, *53*(12), 1012–1016. https://doi.org/10.1130/G53481.1

Taylor, W. R. (1998). An experimental test of some geothermometer and geobarometer formulations for upper mantle peridotites with application to the thermobarometry of fertile lherzolite and garnet websterite. *Neues Jahrbuch fuer Mineralogie, Abhandlungen*, *172*(2–3), 381–408. https://doi.org/10.1127/njma/172/1998/381

Tomlinson, E. L., & Kamber, B. S. (2021). Depth-dependent peridotite-melt interaction and the origin of variable silica in the cratonic mantle. *Nature Communications*, *12*(1), 1082. https://doi.org/10.1038/s41467-021-21343-9

Wang, H., van Hunen, J., Pearson, D. G., & Allen, M. B. (2014). Craton stability and longevity: The roles of composition-dependent rheology and buoyancy. *Earth and Planetary Science Letters*, *391*, 224–233. https://doi.org/10.1016/j.epsl.2014.01.038

Zheng, J. P., Lee, C. T., Lu, J. G., Zhao, J. H., Wu, Y. B., Xia, B., et al. (2015). Refertilization-driven destabilization of subcontinental mantle and the importance of initial lithospheric thickness for the fate of continents. *Earth and Planetary Science Letters*, *409*, 225–231. https://doi.org/10.1016/j.epsl.2014.10.042

References From the Supporting Information

Grütter, H. S., Gurney, J. J., Menzies, A. H., & Winter, F. (2004). An updated classification scheme for mantle-derived garnet, for use by diamond explorers. *Lithos*, *77*(1–4), 841–857. https://doi.org/10.1016/j.lithos.2004.04.012

Putirka, K. D. (2008). Thermometers and barometers for volcanic systems. *Reviews in Mineralogy and Geochemistry*, *69*(1), 61–120. https://doi.org/10.2138/rmg.2008.69.3

19448007, 2025, 24, Downloaded from https://agupubs.onlinelibrary.wiley.com/doi/10.1029/2025GL118856 by Cambridge University Library, Wiley Online Library on [17/12/2025]. See the Terms and Conditions (https://onlinelibrary.wiley.com/terms-and-conditions) on Wiley Online Library for rules of use; OA articles are governed by the applicable Creative Commons License